PCCP

RSC Publishing

PAPER

View Article Online
View Journal | View Issue

Cite this: *Phys. Chem. Chem. Phys.*, 2013, **15**, 15470

Carbon nanotubes as electronic interconnects in solid acid fuel cell electrodes

Áron Varga,†[a] Moritz Pfohl,†[b] Nicholas A. Brunelli,[c] Marcel Schreier,[b] Konstantinos P. Giapis[b] and Sossina M. Haile*[ab]

Received 27th March 2013,
Accepted 12th July 2013

DOI: 10.1039/c3cp52586d

www.rsc.org/pccp

Carbon nanotubes have been explored as interconnects in solid acid fuel cells to improve the link between nanoscale Pt catalyst particles and macroscale current collectors. The nanotubes were grown by chemical vapor deposition on carbon paper substrates, using nickel nanoparticles as the catalyst, and were characterized using scanning electron microscopy and Raman spectroscopy. The composite electrode material, consisting of CsH_2PO_4, platinum nanoparticles, and platinum on carbon-black nanoparticles, was deposited onto the nanotube-overgrown carbon paper by electrospraying, forming a highly porous, fractal structure. AC impedance spectroscopy in a symmetric cell configuration revealed a significant reduction of the electrode impedance as compared to similarly prepared electrodes without carbon nanotubes.

Introduction

Fuel cells have the potential to play a leading role in a sustainable energy future due to their high efficiency for converting chemical energy into electrical energy.[1–3] Solid acid fuel cells (SAFCs), in particular, are well positioned to fulfill this role because, amongst other attractive features, their intermediate operating temperature ($\sim$240 °C) leads to fuel flexibility and resistance to catalyst poisoning.[4–10] To date, a maximum peak power density of 415 mW cm^{-2} on hydrogen–oxygen has been reported in the open literature with a platinum catalyst loading of 7.7 mg cm^{-2} (per electrode).[7,11] Pre-commercial efforts have led to reductions in the total Pt loading to $\sim$3 mg cm^{-2}, achieved concomitantly with slight increases in the power output.[12] In order to advance SAFC technology towards true commercial viability, however, it is essential to further reduce the Pt loading while maintaining or even increasing power densities.

We pursue here a strategy for attaining this goal that stems from several recent experimental observations and achievements. First, it has been established that the conventional composite electrode in SAFCs, composed of electrolyte particles, Pt nanoparticles, and Pt on graphite, has activity that scales inversely with electrolyte particle size.[13] That is, a reduction in the electrolyte particle size from 1150 nm to 160 nm (with a fixed Pt loading) has led to a monotonic and significant reduction of the electrode overpotential.[13] This is believed to result from an increase in the number density of catalytically active sites within a given volume of electrode material. Second, it has been possible to estimate the inherent or limiting activity for Pt on a per unit mass basis in a dense, thin-film (7.5 nm) electrode geometry.[14] Deviations from the 'ideal' value of the mass-normalized activity of the well-defined structure provide a measure of Pt utilization in composite structures. Third, the catalyst-mass-normalized activity in the finest composite structures we have been able to prepare to date, obtained using the method of electrospray,[15] is substantially lower than the ideal value. This low relative activity suggests that Pt in the composite structure is poorly utilized, which, in turn, may be the result of poor electronic connectivity between Pt nanocatalyst particles and the exterior current collector. That is, despite the reduction in the electrolyte particle size and the creation of a highly porous, fractal electrode with interconnected nanoscale electrolyte particles, a large fraction of the Pt particles are apparently isolated electrically and cannot deliver current.

Here we explore the potential of carbon nanotubes (CNTs) grown directly on the current collector to serve as conductive interconnects that link Pt nanoparticles to the exterior circuit. While the focus is on SAFCs, the approach may be broadly applicable to lower temperature fuel cells. Indeed, the utility of carbon nanotubes as platinum catalyst supports for polymer electrolyte membrane (PEM) fuel cells has been discussed in the recent literature.[16–19] The present study employs CNTs in the anodes of SAFCs as a proof-of-principle for the design strategy of enhanced interconnectivity. Although overpotentials

[a] *Materials Science, California Institute of Technology, USA. E-mail: smhaile@caltech.edu*
[b] *Chemical Engineering, California Institute of Technology, USA*
[c] *Chemical and Biomolecular Engineering, Georgia Institute of Technology, USA*
† These authors contributed equally to this work.

at the cathode are more severe than at the anode of SAFCs[7] (as they are in state-of-the-art PEM fuel cells[20]) the Pt loadings of $\sim$3 mg cm^{-2} in SAFC anodes remain high and substantial reductions in costs can be anticipated by enhancing utilization even for hydrogen electrooxidation. The tendency of Pt to oxidize at the cathodes of SAFCs complicates an analogous study of the effect of well-dispersed current collectors on oxygen electrocatalysis and accordingly is not pursued here.

Experimental methods

Carbon nanotube synthesis

Carbon nanotubes (CNTs) were grown on carbon paper substrates by chemical vapor deposition (CVD) using Ni nanoparticles as the catalyst and acetylene as the gaseous carbon source.[21] Nickel nanoparticles were synthesized following a procedure described by Metin *et al.*[22] In brief, 1.03 g of nickel acetylacetonate was mixed with 60 mL of oleylamine and 1.2 mL of oleic acid in a nitrogen environment. Moisture and oxygen were removed from this solution by heating it to 110 °C and holding at that temperature for one hour. Separately, 1.06 g of the borane tributylamine complex was dissolved in 8 mL of oleylamine. The nickel-containing solution was cooled to 90 °C and the second solution rapidly injected into it to induce the reduction of nickel acetylacetonate by borane tributylamine. The reaction was allowed to proceed for 60 min. After cooling to room temperature, the organic products were removed by adding 120 mL of ethanol, centrifuging (3000 rpm for 10 min), and then decanting. The resulting oleylamine-capped particles were then re-dispersed in hexane. Typical particle sizes obtained using this method are 3.2 nm.[22] Immediately prior to dispensing on the carbon paper, the suspension was subjected to ultra-sonication for one hour to encourage the break-up of agglomerates. The catalyst particles were applied to the carbon paper substrates (Toray-H-120, 5 × 5 mm^2 in area) by spin coating. Two drops of the solution were dispensed to each substrate as it was spun at 2000 rpm for 15 s, resulting in a catalyst loading of $\sim$0.25 mg cm^{-2}.

The catalyst-loaded substrate was then placed in the center of an in-house CVD reactor consisting of a quartz tube (2.5 cm dia. and 61.5 cm length), a tube furnace (Lindberg/Blue M Mini-Mite, monitored using a K-type thermocouple), and mass flow controllers, Fig. 1. The details of the growth protocol employed (typical of procedures reported in the literature[21]) are given in Table 1. The initial heating to 800 °C was carried out under argon and followed by 10 min annealing under a mixture of hydrogen and argon to ensure the reduction of any NiO to Ni. The oleylamine, with a boiling point much lower than 800 °C,[23,24] is presumably volatilized before or during the annealing step, although some carbon may be incorporated into the catalyst particles during these stages. The 10 min growth step was carried out under a mixture of acetylene, hydrogen, and argon. The sample was subsequently cooled under argon flow.

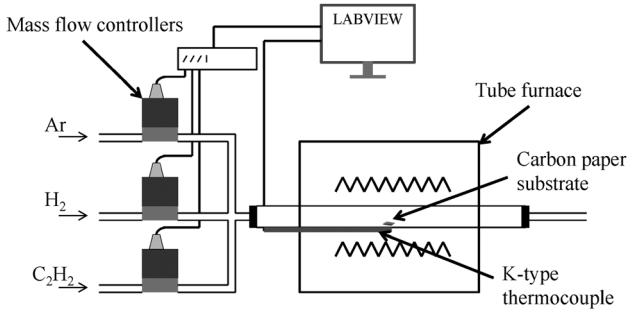

Fig. 1 CVD apparatus for CNT growth.

Table 1 Conditions for CVD growth of CNTs used in electrodes of solid acid fuel cells

	Ramp	Anneal	Grow	Cool
Temperature (°C)	20 → 800	800	800	800 → 20
Ramp rate (°C min^{-1})	15	0	0	Passive
Time (min)	52	10	10	30
Argon (sccm)[a]	750	750	750	750
Hydrogen (sccm)	0	250	250	0
Acetylene (sccm)	0	0	16	0

[a] sccm = standard (standard temperature and pressure) cubic centimeters per minute.

Electrode fabrication

Composite electrodes comprising CsH_2PO_4 and Pt were deposited on carbon paper substrates by electrospray using methods described by Varga *et al.*[15] Both neat (as-purchased) and CNT-overgrown carbon paper substrates were employed. In addition, two different electrospray solutions were utilized, the compositions of which are detailed in Table 2. Both contained dissolved CsH_2PO_4 as well as dispersed Pt, where the latter was a combination of both Pt black (Alfa Aesar Stk# 43 838; estimated particle diameter of $\sim$10 nm) and Pt on carbon (Alfa Aesar Stk# 42 204; manufacturer-reported Pt particle diameter of $\sim$5 nm). The CsH_2PO_4 was synthesized in-house using Cs_2CO_3 (Alfa Aesar, 99% metal basis, Stk# 12 887) and H_3PO_4 (Mallinckrodt Chemicals, 85%, Stk# 2788-14) as precursors. The two solutions differed in the Pt content (with the ratio of Pt black to Pt on carbon held constant), which was varied as a means of probing the effectiveness of the CNTs for providing current collection pathways at different Pt loadings. Polyvinylpyrrolidone (PVP) was added in both cases to aid in the suspension of the Pt and carbon solid components, and the PVP-to-solids weight ratio was also held constant between the two solutions. As a control, a solution of CsH_2PO_4 and PVP (but no Pt) was electrosprayed on the CNT-overgrown carbon paper to assess the possible contribution of CNTs and/or Ni nanoparticles to any observed catalytic activity.

As in our previous work,[15] the electrospray chamber was operated at ambient pressures, the temperature was fixed at 140 °C (to facilitate solvent evaporation), the voltage between the capillary tip and the substrate was 4.5 kV, the tip to substrate distance was 2.5 cm, the nitrogen sheath gas velocity was 67 cm min^{-1}, the liquid flow rate was 1 mL h^{-1}, and deposition was carried out for 1 hour. The quantity of material deposited onto the substrate was determined from a comparison of the pre- and post-deposition weights, as measured using a micro-balance, from which the Pt loading was computed. In continued

Table 2 Electrospray solution composition

	Solution 1	Solution 2[a]	Control
CsH_2PO_4 (g L^{-1}) (in-house)	10	10	10
Platinum black (g L^{-1}) Alfa Aesar, Stk # 43 838, $\sim$30 m^2 g^{-1}	3	5	0
Platinum (40 wt%) on carbon[b] (g L^{-1}) Alfa Aesar, Stk #42 204	3	5	0
Polyvinylpyrrolidone (g L^{-1}) Alfa Aesar, Stk#41 626 M_W 8000 u	12	20	20
Deionized water–methanol (wt%) macron chemicals, 3016-16	50	50	50

[a] Composition matches that used in a previous study.[15] [b] Vulcan XC-72R.

analogy to our earlier study, for control electrodes not containing CNTs, an oxygen plasma treatment step (150 W power, 13.56 MHz frequency, 13.6 mTorr Ar + O_2 mixture, 4 min exposure) was employed in order to remove PVP,[15] which could otherwise coat the Pt catalyst particles and prevent electrochemical access. In the case of the CNT-containing electrodes, the oxygen plasma treatment step was omitted to avoid possible damage to the carbon structures.

Electrochemical characterization was performed on symmetric cells configured as follows: carbon paper:composite electrode $|CsH_2PO_4|$ composite electrode:carbon paper.

A disk of the electrolyte material (1.9 cm diameter and 1–2 mm thick) of $\sim$95% density was first obtained by uniaxially pressing (34 MPa). Two electrodes, each $\sim$2 mm^2 in area, were cut out from a given substrate and positioned in the middle of either side of the flat electrolyte pellet. The sandwich structure was then lightly pressed between inactive carbon paper current collectors.

Characterization

The morphological features of the samples were characterized using a scanning electron microscope (Zeiss 1550VP and Hitachi S-4100 field emission SEM) equipped with a secondary electron detector. The as-grown CNTs were further characterized using Raman spectroscopy (Renishaw M1000 Micro Raman Spectrometer System).

A.C. impedance spectra were collected at 240 °C under humidified hydrogen as a means of probing the hydrogen electro-oxidation reaction. Hydrogen gas (> 99.95% purity) was bubbled through water held at 80 °C to achieve a water partial pressure of 0.4 atm and supplied at a gas phase velocity of 3.1 cm min^{-1}. Electrical data were acquired using an impedance analyzer (Autolab PGSTAT 32) over the frequency range 5 mHz to 1 MHz, a perturbation voltage amplitude of 10 mV, and zero D.C. bias. Two different and four different cells created from solutions 1 and 2, respectively, with CNT-modified electrodes were characterized. Stability was evaluated by collecting data over 8–12 h periods. Impedance data are reported as normalized with respect to the area of the carbon paper electrode over which CNTs were grown (active area). The current–voltage characteristics of a representative CNT-containing symmetric cell, created from solution 2, were evaluated *via* linear sweep cyclic voltammetry. The voltage was varied from +0.5 to −0.5 V at a sweep rate of 5 mV s^{-1}, and impedance spectra collected at selected values of fixed bias. As with the unbiased impedance measurements, data were obtained at 240 °C under humidified hydrogen (pH_2O = 0.4 atm). The results from impedance spectroscopy measurements under bias were used to separate the electrolyte and electrode contributions to the total cell voltage.

Results and discussion

Images of the carbon paper substrate after CNT growth are presented in Fig. 2. The regions of the carbon paper where nickel nanoparticles had been deposited acquired a uniform black appearance, demonstrating the effectiveness of these particles in catalyzing CNT growth, Fig. 2a. Energy dispersive spectroscopy confirmed the general presence of Ni in these regions. Other areas of the carbon paper retained the grey appearance of the as-purchased substrate. Within the regions of CNT growth, the coverage over the carbon paper is visually uniform, Fig. 2b and c. The diameter of the CNTs ranges from 15 to 25 nm and they extend out $\sim$8 μm from the surface of the carbon paper fiber. In some images (not shown) in which the tip of the CNT was visible, the CNT was terminated by a bright spot, consistent with the presence of Ni and the tip growth mechanism.[25] However, exhaustive imaging was not performed that would rule out the base growth mechanism. In general, whether formed by tip or base growth, the diameter of a CNT is comparable to the size of the catalyst particle from which it grows. Here, the observed CNT diameters are larger than the 3.2 nm expected from the Ni synthesis, suggesting that coarsening may have occurred during the high temperature annealing prior to CNT growth. Images of similarly prepared Ni particles annealed

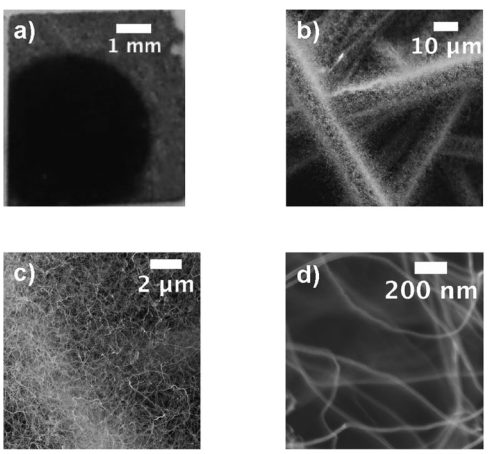

Fig. 2 Images of as-grown CNTs on the carbon paper: (a) optical image; and (b–d) scanning electron microscopy images.

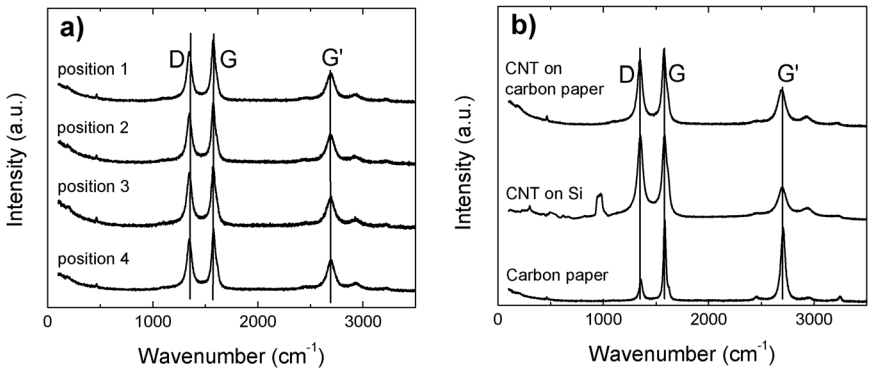

Fig. 3 Raman spectra of as-grown CNTs on various substrates. (a) Spectra from four different positions of a single carbon paper substrate, and (b) comparison of spectra as indicated.

at 550 °C for 10 min under Ar revealed agglomerates 10–40 nm in diameter formed of 3.9 nm primary particles.[26] The large diameter of the CNTs further suggests that they are multi-walled.[27] In contrast to the diameter, the length of a CNT is dictated by the growth time before the catalyst loses activity.[25] Consistent with this inherent behavior, growth periods longer than 10 min did not result in longer CNTs.

Raman spectra of the CNTs are presented in Fig. 3. The spectra in Fig. 3a correspond to measurements from four different areas chosen randomly on a single substrate and are normalized with respect to the peak intensity of the G-band. The four spectra are nearly identical and corroborate the electron microscopy observation of generally uniform CNT growth across the substrate. A CNT sample, removed from the carbon paper substrate by ultra-sonication in ethanol and deposited on a Si wafer, had a Raman spectrum almost identical to that obtained from the CNT on the carbon paper, Fig. 3b. These two spectra (detached CNTs on Si and attached CNTs on the carbon paper) are, however, clearly distinct from that of the carbon paper alone, indicating that the attached CNTs on the carbon paper largely, if not fully, mask the underlying substrate. The spectra of the attached CNTs are, in particular, distinguished from that of the substrate by the high intensity of the D band, consistent with the presence of highly graphitic carbon in the former.[28] The absence of a peak in the 100 to 300 cm^{-1} range, at which the radial breathing mode would be observed, is typical of multi-walled CNTs.[29]

Upon electrospraying on the carbon paper current collectors for a period of *ca.* 120 min, solutions 1 and 2 (Table 2) yielded composite electrodes with estimated Pt loadings of 0.2 mg cm^{-2} and 0.3 mg cm^{-2}, respectively. These electrodes acquired differing morphologies depending on the presence or the absence of the CNTs. As evident from the SEM images, Fig. 4, the porosity was somewhat lower for deposition on substrates with CNTs. While the images presented in Fig. 4 are for solution 1, similar results were obtained for solution 2. At this stage the reason for the distinct morphologies is unknown.

Fig. 5 shows the impedance spectra in the Nyquist representation ($-Z_{imag}$ *vs.* Z_{real} as parametric functions of frequency) for symmetric cells fabricated with solution 1 (lower platinum loading) after a 3–8 hours initial equilibration time. The data

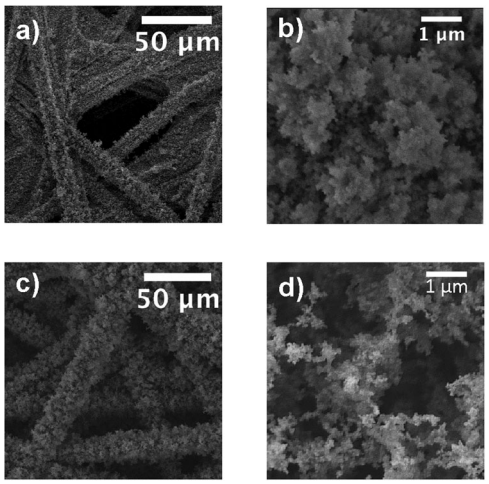

Fig. 4 SEM images of the electrosprayed composite electrodes, consisting of CsH_2PO_4, platinum black, platinum on carbon black and polyvynilpyrrolidone deposited onto the carbon paper (a and b) with and (c and d) without CNTs at low and high magnification respectively.

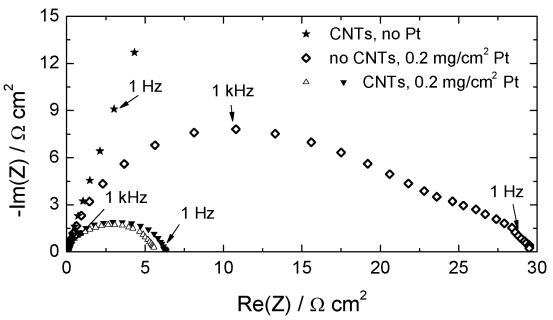

Fig. 5 Impedance spectra of two composite electrodes with CNTs and one without, but otherwise identical (solution 1 with lower platinum loading, as indicated).

presented are those obtained once the change in electrode impedance fell below a rate of 4% per hour. For clarity, the electrolyte contribution, a constant displacement along the real axis, is subtracted from the data. Cells with both CNTs and Pt in the electrodes showed a five-fold reduction of the electrode

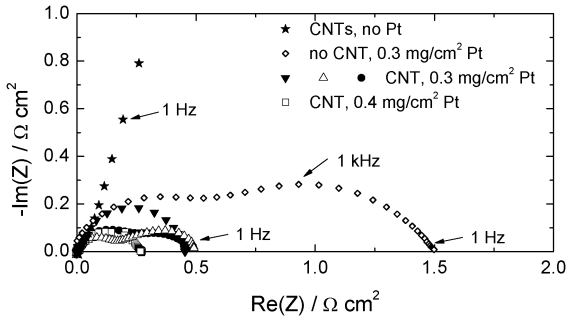

Fig. 6 Impedance spectra of four composite electrodes with CNTs and one without but otherwise identical (solution 2 with higher platinum loading, as indicated).

impedance as compared to those with only Pt (6 Ω cm^2 *vs.* 30 Ω cm^2). Furthermore, excellent reproducibility is evident for the two different cells with electrodes containing both CNTs and Pt. A similar result, also after a 3–8 hours initial equilibration time, was obtained in the case of cells fabricated using solution 2 (higher Pt loading), Fig. 6. In this case, however, the presence of CNTs leads to a three-fold decrease in impedance (0.5 Ω cm^2 *vs.* 1.5 Ω cm^2). Again, reproducibility is high, and the results for the cell with Pt but no CNTs match previously reported results.[15] Moreover, the enhancement obtained using the CNT-modified carbon paper occurs despite the potential presence of residual PVP, which has been shown to have a slight negative impact on activity.[15] Overall, the low impedance values obtained in the presence of the CNTs directly translate into five- and three-fold improvements in the catalyst utilization, respectively. Specifically, the mass normalized activity [inverse of (area normalized electrode impedance × Pt loading)] was increased from 0.2 to 1.0 S mg^{-1} for the lower Pt loading and from 2.2 to 6.6 S mg^{-1} for the higher Pt loading.

In the absence of Pt, the CNT-modified electrode displayed negligible activity, as shown in both Fig. 5 and 6. Thus, neither the CNTs nor the residual (carbon-saturated) Ni can be responsible for the observed enhancement over Pt-only electrodes when both CNTs and Pt are present. Furthermore, although the possibility of a synergistic interaction between Ni and Pt cannot be ruled out, the relatively low fabrication (electrospray deposition) and measurement temperatures suggest that these two types of particles remain as discrete units, with little likelihood of interdiffusion even where they do come into contact.

The observations of substantially enhanced activity in CNT + Pt electrodes over those with Pt only and of negligible activity for electrodes with only CNTs suggest strongly that the CNTs are providing the desired electrical contacts to the Pt catalyst particles. The greater impact of the CNTs at the low Pt loading (a five-fold improvement *vs.* a three-fold improvement at high Pt loading) is consistent with the occurrence of a greater fraction of electrically isolated catalyst particles when the amount of Pt is low. The CNT overgrowth on the carbon paper thus provides a larger benefit for lower platinum catalyst loading.

Beyond improved activity, the CNT modified electrodes displayed good stability. The electrode impedance either decreased over time

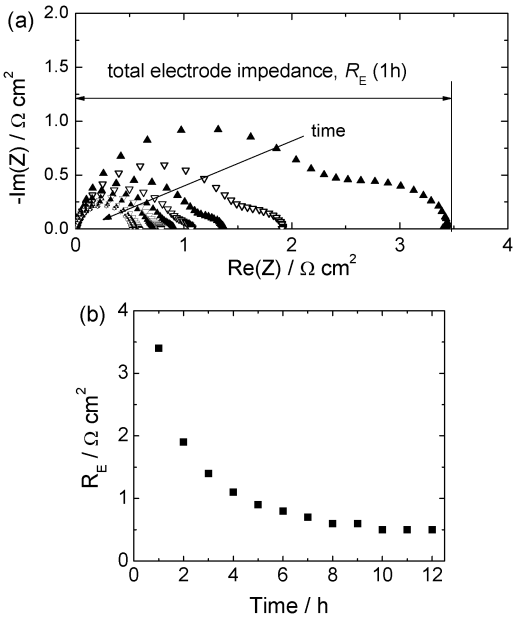

Fig. 7 Impedance of a composite electrode with CNTs (solution 2, 0.3 mg Pt cm^{-2}) taken over a 12 hours period, showing good stability after improvement over an initial 8 hours period: (a) Nyquist representation of data collected hourly and (b) extracted total electrode impedance. Data normalized to the active area of the carbon paper electrode.

to a stable value or remained unchanged during the course of evaluation. An example of the former behavior is shown in Fig. 7, which summarizes measurements for an electrode prepared using solution 2 (higher Pt loading). Two electrode impedance responses are evident for this cell, as reflected by the presence of two arcs in the Nyquist plot, Fig. 7a, a feature generally present in all of the electrodes examined (Fig. 5 and 6). Both arc widths decrease substantially with time to reach stable values after about 8 hours. While the physical origin of the two distinct responses is unknown, we attribute the overall decrease in the global impedance, Fig. 7b, to either an improvement of the contact between the electrosprayed CsH_2PO_4 particles of the composite electrode and the pre-pressed CsH_2PO_4 pellet serving as the electrolyte, or to the volatilization of residual PVP during high temperature exposure. The eventual stabilization of the electrochemical response suggests that after a moderate period of exposure to the light pressure of the electrochemical measurement apparatus the morphology of the electrode/electrolyte interface adopts a fixed configuration, and/or that the process of PVP removal is completed.

The D.C. polarization curve, Fig. 8, reveals that the electrode has an almost ohmic (linear) response. Here, the electrode overpotential is obtained by subtracting from the total measured voltage the ohmic contribution of the electrolyte as determined using impedance spectroscopy (inset). The linearity of the response is reflected not only in the shape of the polarization curve, but also in the features of the impedance spectra, which reveal the electrode impedance to be largely unchanged even at a total cell voltage of 0.5 V (electrode overpotential of ~380 mV). For conventional Butler–Volmer behavior, the *I–V* curve would

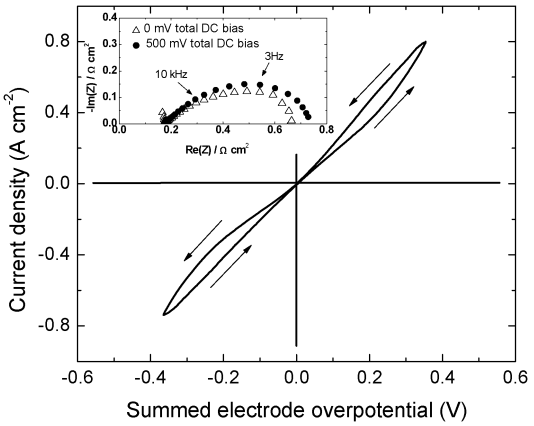

Fig. 8 *I–V* curve of a representative symmetric cell with CNT containing electrodes measured using linear sweep cyclic voltammetry (0.05 V s^{-1} sweep rate) and corresponding impedance spectra without and with DC bias. Current normalized to the active area of the carbon paper electrode. Voltage at electrodes is computed by subtracting ohmic drop across the electrolyte, as determined from the impedance spectra (inset) from the total measured voltage.

show an exponential increase in current with increasing electrode overpotential. A similar pseudo-linear response has been reported previously for SAFC electrodes composed of mechanically milled CsH_2PO_4 and Pt measured under similar conditions.[30] In that case, however, consistent with the much higher electrode resistance obtained in the absence of CNT current collectors, the current was much lower. For example, at an electrode overpotential of about 0.05 V, the current density was just $\sim$25 mA cm^{-2}. Here, if roughly half the overpotential is assigned to each electrode, the corresponding current density is $\sim$200 mA cm^{-2}, an eight-fold increase. The D.C. results thus provide another indicator of the value of CNTs in reducing overpotentials in SAFC electrodes. The results further indicate that the electrodes employed here are active for proton reduction (*i.e.*, hydrogen evolution) in addition to being active for hydrogen electro-oxidation, as neither step (oxidation nor reduction) can incur a voltage penalty greater than the summed electrode overpotential of Fig. 8.

Conclusion

Direct growth of carbon nanotubes onto the current collector (carbon paper) applied to composite electrodes in solid acid fuel cells has resulted in a multi-fold decrease in the electrochemical reaction impedance and a commensurate increase in the Pt utilization relative to similar electrodes without carbon nanotubes. The increased electrode performance is attributed to better catalyst utilization as a result of improved interconnectivity. The CNTs, with diameters of a few nanometers and lengths in the micron range, provide a means of matching the length scales of the Pt catalyst nanoparticles and the micrometric fibers of the carbon paper current collector. Furthermore, the enhanced activity applies to both hydrogen electrooxidation and proton electroreduction (H_2 evolution). While the highest mass normalized activity achieved here, 6.6 S mg^{-1}, is lower than the measured value of 19 S mg^{-1} for Pt thin films,[14] the enhancement over state-of-the-art composite electrodes ($\sim$2.2 S mg^{-1})[7] is substantial. Additional gains may be realized by further optimizing the electrode structure, *e.g.*, by growing longer CNTs and/or ensuring the absence of defects that may have a negative impact on CNT electronic conductivity.

Acknowledgements

This material is based upon work supported by the National Science Foundation under Grant No. DMR-0520565. Funding was also provided by the Gordon and Betty Moore Foundation through the Caltech Center for Sustainable Energy Research and by LiOx corporation. M.P. and M.S. were partially supported by ETH Zurich fellowships. The authors thank Prof. George Rossman for invaluable assistance with Raman spectroscopy measurements. We are also indebted to Prof. Harry Gray, without whose generosity this work would not have been possible.

References

1 S. M. Haile, *Acta Mater.*, 2003, **51**, 5981–6000.
2 J. Larminie and A. Dicks, *Fuel Cell Systems Explained*, Wiley, New York, 2003.
3 B. C. H. Steele and A. Heinzel, *Nature*, 2001, **414**, 345–352.
4 S. M. Haile, D. A. Boysen, C. Chisholm and R. Merle, *Nature*, 2001, **410**, 910–913.
5 S. M. Haile, *Mater. Today*, 2003, 24–29.
6 D. A. Boysen, T. Uda, C. Chisholm and S. M. Haile, *Science*, 2004, **303**, 68.
7 S. M. Haile, C. R. I. Chisholm, K. Sasaki, D. A. Boysen and T. Uda, *Faraday Discuss.*, 2007, **134**, 17.
8 K.-D. Kreuer, *ChemPhysChem*, 2002, **3**, 771–775.
9 T. Norby, *Nature*, 2001, **410**, 877–878.
10 J. Otomo, T. Tamaki, S. Nishida, S. Wang, M. Ogura, T. Kobayashi, C.-j. Wen, H. Nagamoto and H. Takahashi, *J. Appl. Electrochem.*, 2005, **35**, 865–870.
11 T. Uda and S. M. Haile, *Electrochem. Solid-State Lett.*, 2005, **8**, A245.
12 C. R. Chisholm, SAFCell Inc., Personal communication.
13 C. R. I. Chisholm, D. A. Boysen, A. B. Papandrew, S. K. Zecevic, S. Cha, K. A. Sasaki, Á. Varga, K. P. Giapis and S. M. Haile, *Interface Magazine*, 2009, **18**, 53–59.
14 M. W. Louie and S. M. Haile, *Energy Environ. Sci.*, 2011, **4**, 4230.
15 Á. Varga, N. A. Brunelli, M. W. Louie, K. P. Giapis and S. M. Haile, *J. Mater. Chem.*, 2010, **20**, 6309.
16 N. Rajalakshmi, H. Ryu, M. Shaijumon and S. Ramaprabhu, *J. Power Sources*, 2005, **140**, 250–257.
17 H. Tang, J. H. Chen, Z. P. Huang, D. Z. Wang, Z. F. Ren, L. H. Nie, Y. F. Kuang and S. Z. Yao, *Carbon*, 2004, **42**, 191–197.
18 Y. Mu, H. Luiung, J. Hu, L. Jiang and L. Wun, *J. Phys. Chem. B*, 2005, **109**, 22212–22216.
19 X. Wang, M. Waje and Y. Yan, *Electrochem. Solid-State Lett.*, 2005, **8**, A42.
20 H. Gasteiger, S. Kocha, B. Sompalli and F. Wagner, *Appl. Catal., B*, 2005, **56**, 9–15.

21 M. Jung, K. Y. Eun, J.-K. Lee, Y.-J. Baik, K.-R. Lee and J. W. Park, *Diamond Relat. Mater.*, 2001, **10**, 1235–1240.
22 O. Metin, V. Mazumderm, S. Ozkar and S. Sun, *J. Am. Chem. Soc.*, 2010, **132**, 1468–1469.
23 W. Haynes, *CRC Handbook of Chemistry and Physics*, CRC Press, 2013.
24 http://www.sigmaaldrich.com.
25 M. Kumar and Y. Ando, *J. Nanosci. Nanotechnol.*, 2010, **10**, 3739–3758.
26 M. Schreier, in *Chemical and Bioengineering*, ETH Zurich, Zurich, 2012.
27 G. D. Nessim, *Nanoscale*, 2010, **2**, 1306–1323.
28 M. S. Dresselhaus, G. Dresselhaus, R. Saito and A. Jorio, *Phys. Rep.*, 2005, **409**, 47–99.
29 A. Jorio, E. Kaupinnen and A. Hassanien, in *Carbon Nanotubes*, ed. A. Jorio, G. Dresselhaus and M. S. Dresselhaus, Springer Verlag, Berlin, 2008.
30 K. A. Sasaki, Y. Hao and S. M. Haile, *Phys. Chem. Chem. Phys.*, 2009, **11**, 8349–8357.

